

The fermionic King model

Pierre-Henri Chavanis, Mohammed Lemou, Florian Méhats

June 1, 2021

Abstract

We study the fermionic King model which may provide a relevant model of dark matter halos. The exclusion constraint can be due to quantum mechanics (for fermions such as massive neutrinos) or to Lynden-Bell's statistics (for collisionless systems undergoing violent relaxation). This model has a finite mass. Furthermore, a statistical equilibrium state exists for all accessible values of energy $E_{min} \leq E \leq 0$. Dwarf and intermediate size halos are degenerate quantum objects stabilized against gravitational collapse by the Pauli exclusion principle. Large halos at sufficiently high energies are in a gaseous phase where quantum effects are negligible. They are stabilized by thermal motion. Below a critical energy E_c they undergo gravitational collapse (gravothermal catastrophe). This may lead to the formation of a central black hole that does not affect the structure of the halo. This may also lead to the formation of a compact degenerate object surrounded by a hot massive atmosphere extending at large distances. We argue that large dark matter halos should not contain a degenerate nucleus (fermion ball) because these nucleus-halo structures are thermodynamically unstable. We compare the rotation curves of the classical King model to observations of large dark matter halos (Burkert profile). Because of collisions and evaporation, the central density increases while the slope of the halo density profile decreases until an instability takes place. We find that the observations are compatible with a King profile at, or close to, the point of marginal stability in the micro-canonical ensemble. At that point, the King profile can be fitted by the modified Hubble profile that has a flat core and a halo in which the density decreases as r^{-3} . This is qualitatively similar to the Burkert profile. Less steep halos are unstable. Discrepancies between the King model and the observations are interpreted as a result of incomplete relaxation.

1 Introduction

According to contemporary cosmology, the universe is made of about 70% dark energy, 25% dark matter, and 5% baryonic (visible) matter [1]. Thus, the overwhelming preponderance of matter and energy in the universe is believed to be dark, *i.e.* unobservable by telescopes. The dark energy is responsible for the accelerated expansion of the universe. Its origin is mysterious and presumably

related to the cosmological constant or to some form of exotic fluid with negative pressure such as the Chaplygin gas. On the other hand, dark matter is necessary to account for the observed flat rotation curves of galaxies. Its nature is one of the most important puzzles in particle physics and cosmology.

We consider the possibility that dark matter halos are described by the Fermi-Dirac distribution at finite temperature. The Fermi-Dirac distribution may have two origins. First, it corresponds to the statistical equilibrium state of a gas of fermions such as massive neutrinos. These particles are subjected to the Pauli exclusion principle similarly to electrons in white dwarf stars and neutrons in neutron stars. As a result, quantum mechanics can stabilize dark matter halos against gravitational collapse and lead to halo cores instead of r^{-1} density cusps predicted by the cold dark matter (CDM) model [2] but not observed [3]. However, there is a difficulty with this scenario because the time it takes a self-gravitating system with a large number of particles to achieve a statistical equilibrium state is usually very long and exceeds the age of the universe by many orders of magnitude [1]. Therefore, the establishment of a Fermi-Dirac distribution in the whole cluster is not granted. Furthermore, the thermodynamical temperature is expected to be very low so that the cluster would be completely degenerate and appear very different from what is observed (except in the case of dwarf halos). Fortunately, there is another possibility. Dark matter halos may have reached a quasi stationary state (QSS) as a result of a violent relaxation similar to the one imagined by Hénon [4], King [5] and Lynden-Bell [6] for collisionless stellar systems such as elliptical galaxies described by the Vlasov-Poisson system. Coincidentally, the statistical prediction of Lynden-Bell [6] is also a Fermi-Dirac-type distribution function, although the effective exclusion principle is not due to quantum mechanics but to the Liouville theorem. Furthermore, the temperature appearing in Lynden-Bell's distribution is an effective out-of-equilibrium temperature T_{eff} that can be much larger than the thermodynamical temperature. This could account for the value of the temperature inferred from the rotation curves of the galaxies using the Virial theorem. Finally, this collisionless relaxation occurs in a few dynamical times and is much more efficient than the collisional relaxation. In the dilute (non degenerate) limit, which is appropriate to large dark matter halos, the Fermi-Dirac distribution reduces to the Boltzmann distribution.

If dark matter is collisionless, a halo should not evolve anymore after having reached a virialized state. As a result, its central density cannot be very high. In order to be more general, we consider the possibility that the core of dark matter halos is collisional [7]. This seems to be necessary to explain the presence of black holes at the center of dark matter halos [8]. When collisional effects are taken into account, dark matter halos behave similarly to globular clusters. However, the collisions between particles do not correspond to two-body encounters as in globular clusters but rather to collisions similar to those in a gas.¹ On the other hand, in fermionic dark matter halos, the Pauli exclusion principle must

¹The relaxation time due to strong short-range collisions is large (of the order of the Hubble time) but, still, much smaller than the relaxation time due to weak long-range encounters.

be taken into account. As a result, collisions tend to establish a Fermi-Dirac distribution at finite temperature. They also allow the central concentration of the system to evolve in time towards large values.

Self-gravitating systems have a very particular thermodynamics first investigated by Antonov [9] and Lynden-Bell & Wood [10] in relation to collisional stellar systems such as globular clusters made of classical point mass stars. There is no statistical equilibrium state in a strict sense because a self-gravitating system in an infinite domain has no entropy maximum (the isothermal sphere corresponding to the Boltzmann distribution has infinite mass) [1]. Therefore, the statistical mechanics of self-gravitating systems is essentially an out-of-equilibrium problem. The absence of statistical equilibrium state is related to the fact that self-gravitating systems like globular clusters have the tendency to evaporate (see, *e.g.*, Appendix A of Ref. [11]). This is already the case for a non-interacting gas if it is not enclosed within a container. However, evaporation is a slow process and a globular cluster can be found, for intermediate times, in a quasi stationary state close to the Michie-King distribution [12, 13] which is a truncated Boltzmann distribution with parameters slowly changing with time. If we enclose the system within a “box” so as to prevent artificially its evaporation [9, 10], it is found that statistical equilibrium states exist only above a critical energy $E_c = -0.335 GM^2/R$ discovered by Emden [14]. They have a density contrast $\rho(0)/\rho(R) < 709$. These configurations are metastable (local entropy maxima) but their lifetime is considerable since it scales as e^N (except close to the critical point) [15]. For globular clusters, for which $N \sim 10^6$, this lifetime is so large that metastable states can be considered as stable states. For $E < E_c$, there is no statistical equilibrium state. The system undergoes a gravothermal catastrophe [10] and experiences core collapse.

The evolution of a self-gravitating system is a three stages process.² (i) In the collisionless regime, a self-gravitating system initially out-of-equilibrium reaches a quasi stationary state (virialized state) as a result of a violent relaxation [6]. (ii) In the collisional regime, the system follows a sequence of King distributions [12, 13] that are long-lived metastable equilibrium states [15]. The evolution is driven by a slow evaporation. During that stage, the halo expands while the core shrinks and the central density increases as a consequence of the Virial theorem. (iii) When the central density reaches a critical value, the gravothermal catastrophe sets in and the system undergoes core collapse [17, 18, 19]. For classical self-gravitating systems, such as globular clusters, core collapse leads to a binary star surrounded by a hot halo.³ The formation of binaries at the center

²For a recent review on the kinetic theory of stellar systems, emphasizing the pioneering works of Michel Hénon to which this book is dedicated, see Ref. [16].

³This structure, “binary star + hot halo”, can be understood simply in terms of thermodynamics. This is the most probable structure in the microcanonical ensemble (MCE). Indeed, we can increase indefinitely the entropy S of a self-gravitating system at fixed mass and energy by approaching two stars at very close distance and redistributing the released energy in the halo in the form of kinetic energy (see, *e.g.*, Appendix A of [11]). The binary has a small mass $2m \ll M$ but a huge potential energy $E_{binary} \rightarrow -\infty$. Since the total energy E is fixed in MCE, the kinetic energy (temperature) of the halo $T \rightarrow +\infty$ and, consequently, the entropy $S \sim \frac{3}{2} N k_B \ln T \rightarrow +\infty$. Since the halo is “hot”, it has the tendency to extend

of globular clusters was anticipated early by Hénon [20, 21]. These binaries can release sufficient energy to stop the collapse and even drive a re-expansion of the cluster in a post-collapse regime [22]. This is followed by a series of gravothermal oscillations [23, 24]. It is estimated that about 80% of globular clusters are described by the King model while 20% have undergone core collapse. For self-gravitating systems made of fermions (white dwarfs, neutron stars, dark matter halos) the collapse stops when the core of the system becomes degenerate. This leads to a core-halo structure with a dense degenerate nucleus surrounded by a dilute atmosphere. In that case, we can describe phase transitions between a gaseous phase unaffected by quantum mechanics and a condensed phase stabilized by quantum mechanics. These phase transitions have been studied in detail by Chavanis [25] when the system is confined within a box.

In the present paper, we make a step further and consider the fermionic King model which is a truncated Fermi-Dirac distribution [26, 27]. It can be viewed as a generalization of the classical King model to the case of fermions. The fermionic King model can be derived from a kinetic theory (based on the fermionic Landau equation) by assuming that the particles escape the system when they reach a maximum energy [27]. This derivation is valid both for quantum particles (fermions) and for collisionless self-gravitating systems undergoing Lynden-Bell’s form of violent relaxation.

The fermionic King model is interesting from the viewpoint of statistical mechanics [25]. Indeed, because of the energy truncation, this distribution has a finite mass without the need to introduce an artificial box. On the other hand, because of the exclusion constraint (Pauli or Lynden-Bell bound), there exist a strict equilibrium state (global entropy maximum) for all accessible values of energy $E_{min} \leq E \leq 0$. There may also exist metastable states (local entropy maxima) that can be as much, or even more, important than fully stable states.⁴ As we shall see, the nature of phase transitions in the fermionic King model is similar to that already described in [25] for box-confined self-gravitating fermions. However, this model is more physical (since there is no box) and it is therefore interesting to adapt the study of [25] to this more general situation.

The fermionic King model is also interesting from the viewpoint of astrophysics and cosmology because it provides a realistic model of dark matter halos. The possibility that dark matter is made of fermions (*e.g.* massive neutrinos) has been contemplated by several authors (see a detailed list of references in [28]). Recently, de Vega *et al.* [29] have compared fermionic models of dark matter halos with observations and obtained encouraging results. However, they use the usual Fermi-Dirac distribution. Since this distribution has infinite mass, it is not fully realistic to describe dark matter halos. Furthermore, this precludes

at large distances. It can be shown [11] that the divergence of entropy is maximum when the mass in the core is the smallest (*e.g.* a binary).

⁴Indeed, the choice of the equilibrium state depends on a notion of “basin of attraction” and the metastable states may be reached more easily from generic initial conditions than the fully stable states that require very particular correlations. For example, in order to pass from the gaseous phase to the condensed phase the system must cross a huge barrier of entropy and evolve through an intermediate phase in which some particles must approach very close to each other. The probability of such a configuration is extremely low [15, 25].

the possibility of making a stability analysis and describing phase transitions.

In this contribution, we discuss the main properties of the classical and fermionic King models in MCE. We plot the caloric curves and the profiles of density and circular velocity. We study the stability of the solutions by using the Poincaré theory of linear series of equilibria and we describe phase transitions between a gaseous phase and a condensed phase. We also compare our theoretical predictions to the observations of dark matter halos. A more detailed study is developed in [28].

2 The classical and fermionic King models

The fermionic King model is defined by the distribution function [28]:

$$f = A \frac{e^{-\beta(\epsilon - \epsilon_m)} - 1}{1 + \frac{A}{\eta_0} e^{-\beta(\epsilon - \epsilon_m)}} \quad \text{if } \epsilon \leq \epsilon_m, \quad (1)$$

$$f = 0 \quad \text{if } \epsilon \geq \epsilon_m, \quad (2)$$

where $f(\mathbf{r}, \mathbf{v})$ gives the mass density of particles with position \mathbf{r} and velocity \mathbf{v} , $\rho(\mathbf{r}) = \int f(\mathbf{r}, \mathbf{v}) d\mathbf{v}$ gives the mass density of particles with position \mathbf{r} , $\Phi(\mathbf{r})$ is the gravitational potential determined by the Poisson equation $\Delta\Phi = 4\pi G\rho$, η_0 is the maximum accessible value of the distribution function, $\epsilon = v^2/2 + \Phi(\mathbf{r})$ is the individual energy of the particles, β is the inverse temperature, ϵ_m is the escape energy above which the particles are lost by the system, and $\mu \equiv \eta_0/A$ is the degeneracy parameter.

For $\epsilon \ll \epsilon_m$, we can make the approximation $e^{-\beta(\epsilon - \epsilon_m)} \gg 1$ and we recover the Fermi-Dirac distribution $f = \eta_0/(1 + e^{\beta\epsilon + \alpha})$ with $\alpha = \ln(\eta_0/A) - \beta\epsilon_m$ [28]. As recalled in the Introduction, the Fermi-Dirac distribution may have two origins: (i) it describes a gas of fermions at statistical equilibrium in which case $\eta_0 = gm^4/h^3$ is the maximum accessible value of the distribution function fixed by the Pauli exclusion principle (h is the Planck constant, m the mass of the particles, and $g = 2s + 1$ the spin multiplicity of the quantum states); (ii) it results from the violent relaxation of a collisionless system of particles (classical or quantum) as described by Lynden-Bell [6] and worked out by Chavanis and Sommeria [30]. In that case, Eqs. (1) and (2) are valid for the coarse-grained distribution function (usually denoted \bar{f}) and η_0 is the maximum value of the fine-grained distribution function. We shall consider the two possibilities since the distributions are formally the same. In the quantum interpretation $\beta = m/k_B T$, where T is the temperature. In Lynden-Bell's interpretation $\beta = \eta_0/k_B T_{eff}$, where T_{eff} is an effective (out-of-equilibrium) "temperature". In order to unify the notations, we write $\beta = 1/T$ where T has the dimension of an energy.

The fermionic King model was introduced heuristically by Ruffini and Stella [26] as a natural extension of the classical King model to fermions in order to describe dark matter halos made of massive neutrinos. This distribution function was independently introduced by Chavanis [27] where it was derived

from a kinetic equation (the fermionic Landau equation) assuming that the particles leave the system when they reach a maximum energy ϵ_m . The kinetic derivation given in [27] is valid either for quantum particles (fermions) or for collisionless self-gravitating systems experiencing Lynden-Bell's type of violent relaxation.

In the non degenerate limit $\mu \rightarrow +\infty$, we can make the approximation $\frac{A}{\eta_0} e^{-\beta(\epsilon-\epsilon_m)} \ll 1$ and we recover the classical King model

$$f = A \left[e^{-\beta(\epsilon-\epsilon_m)} - 1 \right] \quad \text{if } \epsilon \leq \epsilon_m, \quad (3)$$

$$f = 0 \quad \text{if } \epsilon \geq \epsilon_m. \quad (4)$$

For $\epsilon \ll \epsilon_m$, we can make the additional approximation $e^{-\beta(\epsilon-\epsilon_m)} \gg 1$ and we recover the Boltzmann distribution $f = \eta_0 e^{-(\beta\epsilon+\alpha)}$. The classical King model describes globular clusters and, possibly, large dark matter halos for which degeneracy effects (due to the Pauli exclusion principle for fermions or due to the Liouville theorem for collisionless systems undergoing violent relaxation) are negligible.

The fermionic King distribution (1)-(2) is a critical point of the “entropic” functional

$$S = - \int \left\{ A \left[\left(1 + \frac{f}{A} \right) \ln \left(1 + \frac{f}{A} \right) - \frac{f}{A} \right] + \eta_0 \left[\left(1 - \frac{f}{\eta_0} \right) \ln \left(1 - \frac{f}{\eta_0} \right) + \frac{f}{\eta_0} \right] \right\} d\mathbf{r} d\mathbf{v} \quad (5)$$

at fixed energy $E = \frac{1}{2} \int f v^2 d\mathbf{r} d\mathbf{v} + \int \rho \Phi d\mathbf{r}$ and mass $M = \int \rho d\mathbf{r}$. Indeed, it cancels the first order variations of the constrained entropy, $\delta S - \beta \delta E - \alpha \delta M = 0$, where β and α are Lagrange multipliers associated with the conservation of energy and mass. In the non-degenerate limit, the entropic functional associated with the classical King model (3)-(4) is

$$S = - \int A \left[\left(1 + \frac{f}{A} \right) \ln \left(1 + \frac{f}{A} \right) - \frac{f}{A} \right] d\mathbf{r} d\mathbf{v}. \quad (6)$$

We shall be interested in entropy *maxima* at fixed energy and mass

$$S(E) = \max_f \{ S[f] \mid E[f] = E, \quad M[f] = M \}. \quad (7)$$

As discussed in [31, 28], this variational principle provides a condition of thermodynamical stability in MCE for tidally truncated self-gravitating systems. We could also consider the canonical ensemble (CE) where the temperature T is fixed instead of the energy. In that case, the stable fermionic King distribution is obtained by minimizing the free energy $F = E - TS$ at fixed mass. For self-gravitating systems, the statistical ensembles are inequivalent (see, *e.g.*, the reviews [32, 33, 25]). In this contribution, for conciseness, we restrict ourselves to MCE. This is the most relevant ensemble for dark matter halos that are relatively isolated objects (their energy is approximately conserved).

Finally, we would like to make clear that we consider here the *thermodynamical* stability of the fermionic King distribution. This implies that we are considering the stability of the system with respect to a collisional evolution or with respect to a violent relaxation on the coarse-grained scale (both described by the fermionic Boltzmann or Landau equation). We shall see that the fermionic King distributions are not always thermodynamically stable, and this puts interesting constraints on these distributions. On the other hand, we recall that the fermionic King distributions, and more generally all the distribution functions of the form $f = f(\epsilon)$ with $f'(\epsilon) < 0$, are nonlinearly *dynamically* stable with respect to the Vlasov equation describing a collisionless evolution [34].

3 Thermodynamics of the classical King model

We first consider the thermodynamics of the classical King model that corresponds to the non-degenerate limit $\mu \rightarrow +\infty$. This distribution is appropriate to describe globular clusters and it may also be appropriate to describe large dark matter halos.

The series of equilibria $\beta(-E)$ giving the inverse temperature normalized by the quantity $1/[G^2 M^{4/3} (8\pi\sqrt{2}A)^{2/3}]$ as a function of the energy normalized by the quantity $G^2 M^{7/3} (8\pi\sqrt{2}A)^{2/3}$ is plotted in Fig. 1.⁵ It is parameterized by the concentration parameter $k = \beta[\epsilon_m - \Phi(0)]$ going from 0 to $+\infty$ (see [28] for details). This curve updates the one drawn by Katz [31]. It has a snail-like structure (spiral) similar to the series of equilibria of classical isothermal spheres confined within a box (see, *e.g.*, [25]).⁶ The concentration parameter k increases along the series of equilibria. For small k , the system is equivalent to a polytrope of index $n = 5/2$ [28]. This approximation is valid for $E \rightarrow 0^-$ and $T \rightarrow +\infty$. For large k , the system is similar to the isothermal sphere ($n = +\infty$) and the series of equilibria spirals about the limit point $(E_\infty, \beta_\infty) = (-1.07, 0.731)$. Some density profiles, and the corresponding rotation curves $v_c(r) = \sqrt{GM(r)/r}$, are plotted in Figs. 2-5.

In MCE, there exist equilibrium states only for $E > E_c$ with $E_c = -1.54$ (first turning point of energy). The critical energy E_c is the counterpart of the Emden energy for box-confined isothermal spheres. It corresponds to $k_{MCE} = 7.44$. For $E < E_c$ there is no equilibrium state and the system undergoes a gravothermal catastrophe (see the arrow in Fig. 1). As recalled in the Introduction, in the case of globular clusters, core collapse leads to the formation of a binary star surrounded by a hot halo.⁷

We now investigate the thermodynamical stability of the classical King

⁵Some authors [10, 35] use another normalization that is discussed in [28].

⁶We note, however, that the energy is always negative in the present case. This is a consequence of the Virial theorem for self-confined systems. By contrast, for box-confined isothermal spheres, there is an additional term in the Virial theorem that accounts for the pressure of the system against the boundary. As a result, the energy may be positive.

⁷In CE, the system undergoes an isothermal collapse for $T < T_c$ with $T_c = 0.613$ (first turning point of temperature) corresponding to $k_{CE} = 1.34$. In that case, the isothermal collapse leads to a Dirac peak containing all the mass [11, 38, 25].

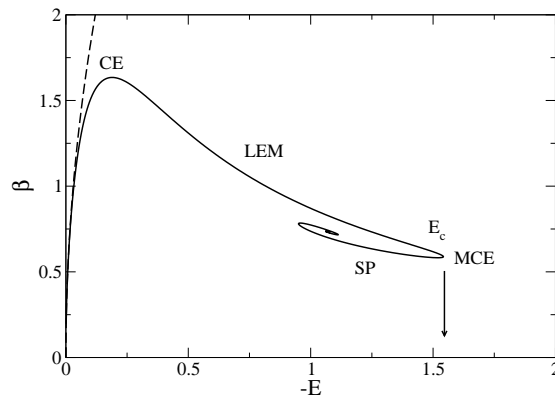


Figure 1: Series of equilibria (parameterized by k) giving the inverse temperature β as a function of the energy $-E$ for the classical King model. The dashed line corresponds to the polytropic approximation.

model according to the optimization problem (7). The stable part of the series of equilibria defines the microcanonical caloric curve.

For $E \rightarrow 0$, the system is stable in MCE since it is equivalent to a polytrope of index $n = 5/2$. Using the Poincaré theory (see, *e.g.*, [39, 25]), we conclude that the series of equilibria is stable until the first turning point of energy MCE and that it becomes unstable after that point. In other words, the King distribution is an entropy maximum (EM) at fixed mass and energy for $k < k_{MCE}$ and a saddle point (SP) of entropy at fixed mass and energy for $k > k_{MCE}$. Since the series of equilibria always rotates clockwise, a mode of stability is lost at each turning point of energy, so the system is more and more unstable as k increases.⁸ Since there is no global entropy maximum at fixed mass and energy for classical self-gravitating systems (see footnote 3), the configurations with $k < k_{MCE}$ are only metastable (local entropy maxima LEM). However, the probability to cross the barrier of entropy and leave a metastable state scales as e^{-N} [15, 25]. For globular clusters for which $N \sim 10^6$ this probability is totally negligible. Therefore, in practice, metastable states are stable states. In this sense, globular clusters can be at statistical equilibrium, described by the King distribution with $k < k_{MCE}$, even if there is no equilibrium state in a strict sense. Their lifetime is controlled by evaporation and core collapse as recalled in the Introduction [1].

⁸There exist a region of ensemble inequivalence between points CE and MCE in Fig. 1, *i.e.* for configurations with $k_{CE} < k < k_{MCE}$ where $k_{CE} = 1.34$ and $k_{MCE} = 7.44$. This part of the series of equilibria is stable in the microcanonical ensemble (entropy maxima at fixed mass and energy) but unstable in the canonical ensemble (saddle points of free energy at fixed mass). It corresponds to configurations with negative specific heats $C = dE/dT < 0$. We know that such configurations are forbidden in the canonical ensemble while they are allowed in the microcanonical ensemble. These results are very similar to those obtained for box-confined isothermal spheres (see, *e.g.*, [32, 33, 25] for reviews).

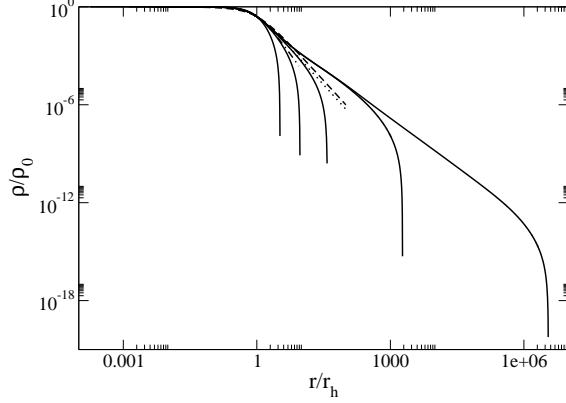


Figure 2: Normalized density profiles of the classical King model in logarithmic scales for (left to right): $k = 1.34$ ($E = -0.188$, $\beta = 1.63$), $k = 5$ ($E = -0.965$, $\beta = 0.893$), $k = 7.44$ ($E = -1.54$, $\beta = 0.589$), $k = 15$ ($E = -1.09$, $\beta = 0.735$), and $k = 30$ ($E = -1.07$, $\beta = 0.732$). We have defined the halo radius r_h such that $\rho(r_h)/\rho_0 = 1/4$ [29]. For $k \rightarrow +\infty$, the system approaches the classical isothermal sphere and the density decreases as r^{-2} with damped oscillations superimposed [36]. However, our study shows that the King profiles with $k > k_{MCE} = 7.44$ are thermodynamically unstable. Therefore, these oscillations may not be physically relevant. As k decreases, the effective slope of the density profile increases. For $k = k_{MCE} = 7.44$ the density profile decreases approximately as $r^{-\alpha}$ with an effective slope $\alpha \sim 3$. For $k = 5$ the density profile has an effective slope $\alpha \sim 4$. The King model is stable in MCE as long as the effective slope α is approximately larger than 3. The dotted line represents the modified Hubble profile which has a slope $\alpha = 3$ [1]. It fits well the core of the isothermal sphere for $r < 1.63r_h$. It also fits well the King model with $k \sim k_{MCE}$ up to $\sim 5r_h$. The dashed-dotted line represents Hénon's isochrone profile that has a slope $\alpha = 4$ [37]. It fits well the King model with $k \sim 5$ up to $\sim 2r_h$. The dashed line represents the Burkert profile corresponding to the observations of dark matter halos [3]. It has a slope $\alpha = 3$.

In Fig. 6 we plot the entropy S normalized by M as a function of the energy $-E$. Since $\delta S = \beta \delta E$ (for a fixed mass M) in MCE, we find that $S(k)$ is extremum when $E(k)$ is extremum. This explain the “spikes” observed in Fig. 6. The series of equilibria becomes unstable after the first spike. This is in agreement with the fact that the states on the unstable branches (after the first spike) have lower entropy than the states on the stable branch (before the first spike) for the same energy.

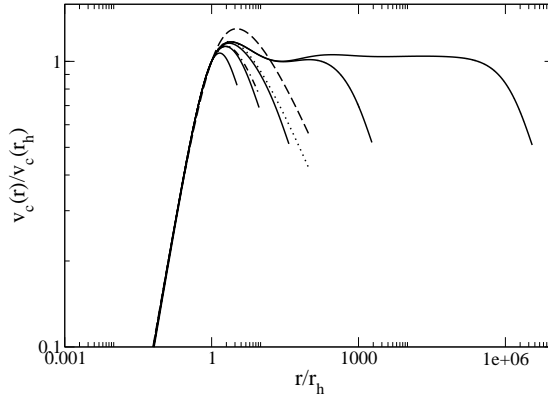


Figure 3: Normalized rotation curves of the classical King model in logarithmic scales for (left to right): $k = 1.34, 5, 7.44, 15$, and 30 . For $k \rightarrow +\infty$, the system approaches the classical isothermal sphere and the rotation curve presents a plateau with damped oscillations superimposed. However, these oscillations occur at very large distances $r > 100r_h$ (probably not accessible observationally) and our study shows that the King profiles with $k > k_{MCE} = 7.44$ are unstable. Therefore, these oscillations may not be physically relevant. For $k \sim k_{MCE}$, the rotation curve presents a maximum close to the halo radius r_h before decreasing, in qualitative agreement with the observational Burkert profile (dashed line). The modified Hubble profile (dotted line) and Hénon's isochrone profile (dashed-dotted line) provide a good fit of the King profiles with $k \sim k_{MCE}$ and $k \sim 5$ respectively up to the tidal radius.

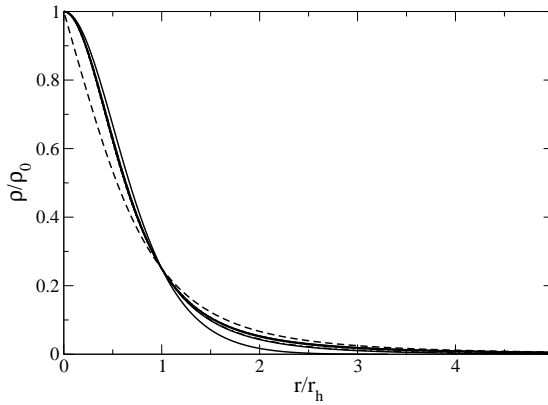


Figure 4: Normalized density profiles of the classical King model in linear scales for (bottom to top): $k = 1.34, 5, 7.44, 15$, and 30 .

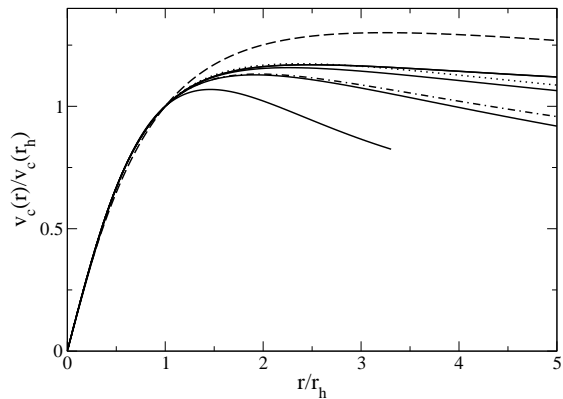


Figure 5: Normalized rotation curves of the classical King model in linear scales for (bottom to top): $k = 1.34, 5, 7.44, 15$, and 30 .

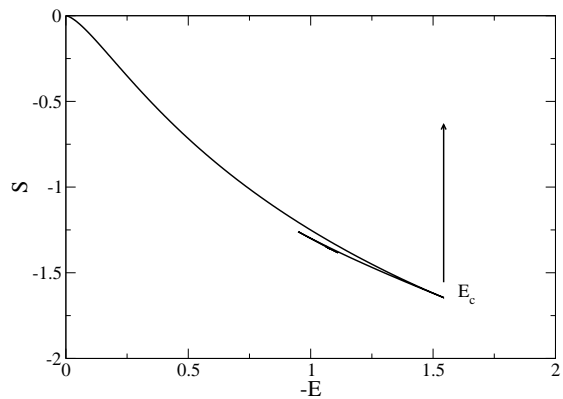


Figure 6: Entropy versus energy for the classical King model.

4 Comparison with the observations of dark matter halos

The fermionic King model provides a realistic model of dark matter halos made of massive neutrinos. Large dark matter halos are non-degenerate and the classical King model can be used. Figs. 2-5 compare the prediction of the King model with the empirical Burkert profile [3]:

$$\frac{\rho(r)}{\rho_0} = \frac{1}{(1+x)(1+x^2)}, \quad x = \frac{r}{r_h}, \quad (8)$$

that fits a large variety of dark matter halos. We see that the Burkert profile is relatively close to the King profile at, or close to, the limit of microcanonical

stability $k_{MCE} = 7.44$. This agreement may be understood as follows. Because of collisions and evaporation, the concentration parameter $k(t)$ increases with time while the slope $\alpha(t)$ of the halo profile decreases until an instability takes place [17]. Therefore, we expect that the halos that have not collapsed have a value of k close to its maximum stable value k_{MCE} , corresponding to a slope $\alpha \sim 3$. At that point, the King profile can be fitted by the modified Hubble profile [1]:

$$\frac{\rho(r)}{\rho_0} = \frac{1}{[1 + (4^{2/3} - 1)x^2]^{3/2}}, \quad x = \frac{r}{r_h}. \quad (9)$$

It has a flat core and a halo in which the density decreases as r^{-3} . These properties are qualitatively similar to the properties of the Burkert profile.

Therefore, the King model gives a relevant description of dark matter halos without fitting parameter. Furthermore, the marginal King profile is physically justified contrary to the Burkert profile that is purely empirical. If we compare the Burkert profile and the marginal King profile more precisely, we see that the agreement is very good in the core for $r \leq r_h$. Therefore, it appears that the core of dark matter halos is isothermal.⁹ We note that the classical King model, which is a truncated isothermal sphere, produces a flat density profile in the core, instead of a cusp, without the need to invoke quantum mechanics. Therefore, warm dark matter (WDM) may account for the absence of density cusps in observations. This thermalisation may be due to collisionless violent relaxation [6, 30], not to collisional relaxation, as explained in the Introduction.

The agreement with the observed rotation curves of galaxies is less good in the halo for $r \geq r_h$. This discrepancy may be interpreted as a result of an incomplete relaxation, as in the case of stellar systems [6]. Therefore, the cores of dark matter halos seem to be isothermal but deviations appear in the halo. The same observation is made for elliptical galaxies. As a whole, these considerations show that statistical mechanics provides a good starting point to understand the structure of dark matter halos but that more work remains to be done in order to obtain a complete picture.

5 Thermodynamics of the fermionic King model

We now consider the thermodynamics of the fermionic King model for arbitrary values of the degeneracy parameter μ . This distribution function is appropriate to describe dark matter halos of various sizes if they are made of massive neutrinos or have experienced violent relaxation.

When an exclusion constraint is taken into account (in the sense of Pauli or in the sense of Lynden-Bell), the structure of the series of equilibria $\beta(E)$ depends on the value of the degeneracy parameter μ as shown in Fig. 7. The degeneracy parameter μ is a measure of the size of the system [28]. Large values of μ correspond to large halos and small values of μ correspond to small halos.

⁹We must be careful, however, because many models of dark matter halos give a good agreement with the Burkert profile for $r < r_h$.

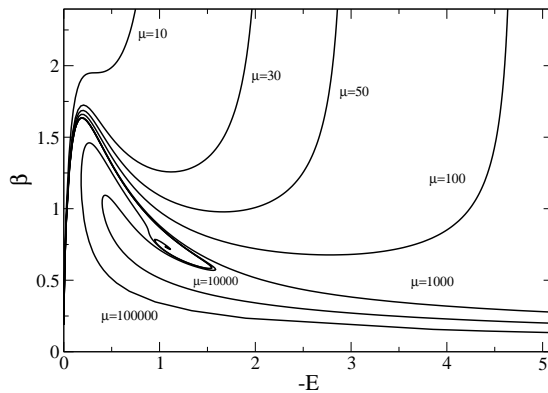


Figure 7: Series of equilibria corresponding to the fermionic King model for different values of the degeneracy parameter μ (note that for large values of μ , the minimum energy $E_{min}(\mu)$ corresponding to $T = 0$ is outside the frame of the Figure). For $\mu \gg 1$, the series of equilibria makes several rotations before unwinding.

For $\mu \rightarrow +\infty$ we recover the classical spiral of Fig. 1. However, for smaller values of μ , we see that the effect of the exclusion constraint is to unwind the spiral. Depending on the value of the degeneracy parameter, the series of equilibria can have different shapes.

For $\mu = 10000$ (large halos), the series of equilibria is represented in Fig. 8. It has a Z-shape structure. Since the curve $\beta(E)$ is multi-valued, this gives rise to microcanonical phase transitions. For $k \rightarrow 0$, the series of equilibria is stable. According to the Poincaré theory [39, 25], it remains stable until the first turning point of energy. At that point a mode of stability is lost as the series of equilibria rotates clockwise. However, the stability is re-gained at the second turning point of energy since the series of equilibria rotates anti-clockwise [25].

The solutions on the upper branch are stable (entropy maxima EM). They are non degenerate and have a smooth density profile. They form the “gaseous phase” (see solution *A* in Figs. 9 and 10). The solutions on the lower branch are also stable (entropy maxima EM). They have a core-halo structure consisting of a degenerate nucleus surrounded by a dilute “atmosphere”. They form the “condensed phase” (see solution *C* in Figs. 9 and 10). The solutions on the intermediate branch are unstable (saddle points of entropy SP). They are similar to the solutions of the gaseous phase but they contain a small embryonic degenerate nucleus playing the role of a “germ” in the theory of phase transitions (see solution *B* in Figs. 9 and 10). These solutions form a barrier of entropy that the system has to cross in order to pass from the gaseous phase to the condensed phase, or inversely (see Ref. [25] for more details).

If we compare the entropy of the solutions (see Fig. 11), we expect a first order microcanonical phase transition to take place at a transition energy $E_t(\mu)$

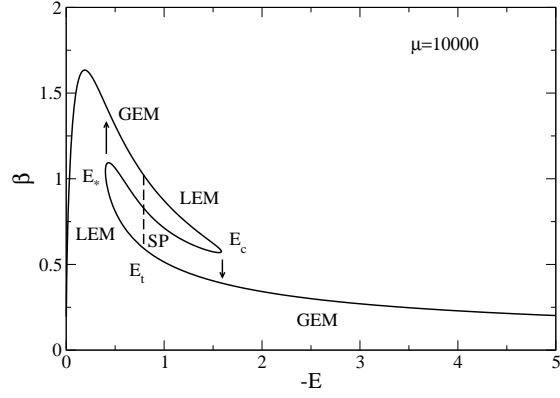


Figure 8: Series of equilibria corresponding to the fermionic King model with $\mu = 10000$.

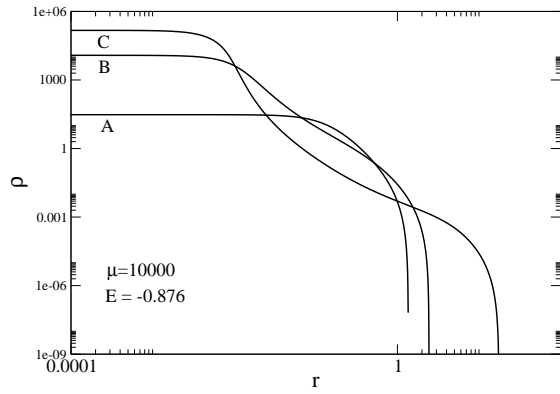


Figure 9: Normalized density profiles corresponding to the different phases of the fermionic King model with $\mu = 10000$ and $E = -0.876$. The radial distance is scaled by $1/(4\pi GM^{1/3}A^{2/3})$ and the density by $(4\pi G)^3 A^2 M^2$. The core-halo structure of solutions B and C comprising a dense degenerate nucleus surrounded by an atmosphere is clearly visible.

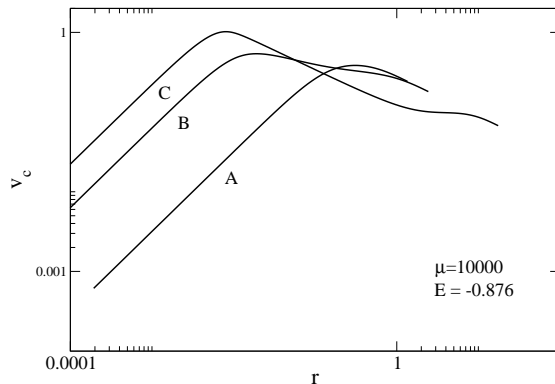


Figure 10: Normalized rotation curves corresponding to the different phases of the fermionic King model with $\mu = 10000$ and $E = -0.876$. The radial distance is scaled by $1/(4\pi GM^{1/3}A^{2/3})$ and the circular velocity by $4\pi GA^{1/3}M^{2/3}$.

where the entropy of the gaseous phase and the entropy of the condensed phase become equal. It is marked by a discontinuity of the inverse temperature $\beta = \partial S/\partial E$ (first derivative of the entropy) in the strict caloric curve. The transition energy $E_t(\mu)$ may also be obtained by performing a Maxwell construction (see the vertical plateau in Fig. 8) [25]. For $E > E_t$, the gaseous phase is fully stable (global entropy maximum GEM at fixed mass and energy) while the condensed phase is metastable (local entropy maximum LEM at fixed mass and energy). For $E < E_t$, the gaseous phase is metastable (LEM) while the condensed phase is fully stable (GEM). However, for systems with long-range interactions, the metastable states have considerably large lifetimes, scaling as e^N , so that the first order microcanonical phase transition does not take place in practice [15, 25]. Therefore, the physical caloric curve must take metastable states into account.

At $E = 0^-$, the system is in the gaseous phase. If we decrease the energy it remains in the gaseous phase until the critical energy $E_c(\mu)$ at which the gaseous phase disappears (spinodal point). For sufficiently large values of μ , this is close to the critical energy $E_c = -1.54$ obtained with the classical King model. For $E < E_c(\mu)$, the system undergoes gravitational collapse (gravothermal catastrophe). However, the collapse stops when the core of the system becomes degenerate (see Fig. 8). In that case, it ends up in the condensed phase. The system has a core-halo structure with a degenerate nucleus surrounded by a non-degenerate atmosphere. Since the collapse is accompanied by a discontinuous jump of entropy (see Fig. 11), this is sometimes called a microcanonical zeroth order phase transition. If we now increase the energy, the system remains in the condensed phase until the critical energy $E_*(\mu)$ at which the condensed phase disappears. For $E > E_*(\mu)$, the system undergoes an “explosion” reversed to the collapse and returns to the gaseous phase (see Fig. 8). In this sense, we have

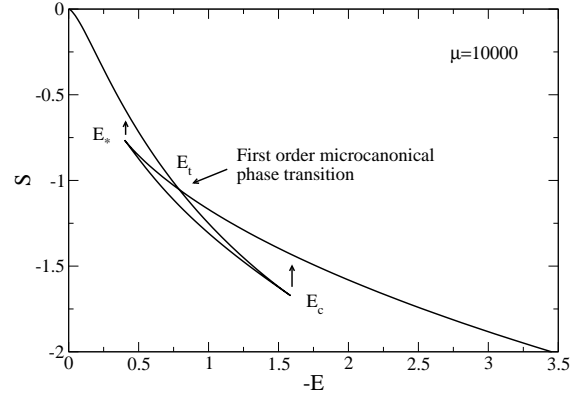


Figure 11: Entropy of each phase versus energy for $\mu = 10000$.

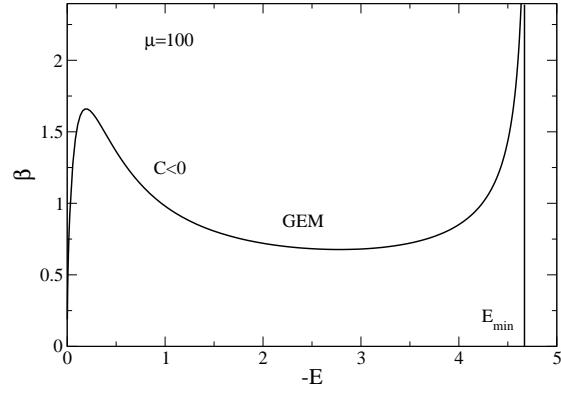


Figure 12: Series of equilibria corresponding to the fermionic King model with $\mu = 100$.

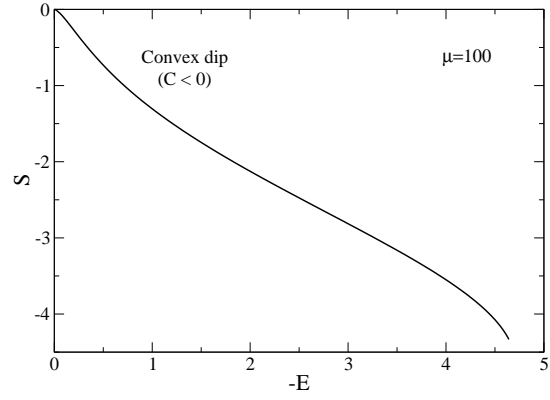


Figure 13: Entropy versus energy for $\mu = 100$.

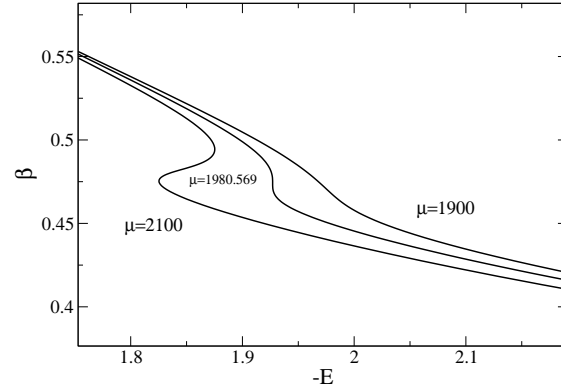


Figure 14: Series of equilibria close to the microcanonical critical point $\mu_{MCP} = 1980$ below which microcanonical phase transitions disappear.

described an hysteretic cycle in the microcanonical ensemble (see the arrows in Figs. 8 and 11).

For $\mu = 100$ (small halos), the series of equilibria is represented in Fig. 12. It has an N -shape structure. Since the curve $\beta(E)$ is univalued there is no phase transition in MCE. All the solutions are fully stable (global entropy maxima GEM at fixed mass and energy), up to the minimum energy E_{min} at which $\beta \rightarrow +\infty$. For intermediate energies, the caloric curve displays a region of negative specific heats ($C = dE/dT < 0$).¹⁰

Another interesting curve is the entropy versus energy relation $S(E)$ represented in Fig. 13. It displays a convex intruder in the region of negative specific heats.

Microcanonical phase transitions occur for $\mu > \mu_{MCP} = 1980$ (microcanonical critical point). They are associated with the turning point of energy at E_c and the multi-valuedness of the series of equilibria $\beta(E)$. For $\mu < \mu_{MCP}$, the series of equilibria $\beta(E)$ unwinds and becomes univalued (see Fig. 14). In that case, there is no microcanonical phase transition (no gravothermal catastrophe) anymore.

6 Density profiles and rotation curves of the fermionic King model

In this section, we discuss in greater detail the structure of the density profiles and of the rotation curves of the fermionic King model.

We first take an energy $E = -0.876 > E_c$ and study the evolution of the solutions A, B and C as μ increases. The series of equilibria is represented in Fig. 15 for $\mu = 10^9$. For $\mu \rightarrow +\infty$, the branches A and B superimpose while the branch C coincides with the $\beta = 0$ axis. As a result, we recover the spiral of Fig. 1.

The solution A (gaseous phase) does not significantly change with μ and tends to the classical King distribution for $\mu \rightarrow +\infty$. The density profile and the rotation curve of the classical King model are represented as dotted lines in Figs. 16-21. Since the classical King model close to E_c describes large dark matter halos relatively well (see Sec. 4) we shall take it as a reference in our discussion.

The solution B (embryonic phase) is similar to the solution A (gaseous phase) except that it contains a small embryonic nucleus. Therefore, the solution B has a nucleus-halo structure. The mass, the size and the absolute value of the potential energy of the nucleus decrease as μ increases. As a result, for large μ , the solutions A and B have almost the same temperature ($\beta_A \simeq \beta_B$) and the profiles A and B coincide outside of the nucleus (see Figs. 16-18). This is why the branches A and B in the series of equilibria superimpose for $\mu \rightarrow +\infty$ (see

¹⁰In CE, this region of negative specific heats is replaced by a canonical phase transition connecting the gaseous phase (left branch) to the condensed phase (right branch) [25, 28].

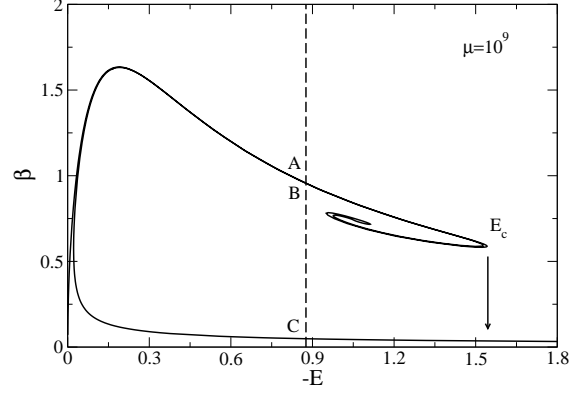


Figure 15: Series of equilibria corresponding to the fermionic King model with $\mu = 10^9$.

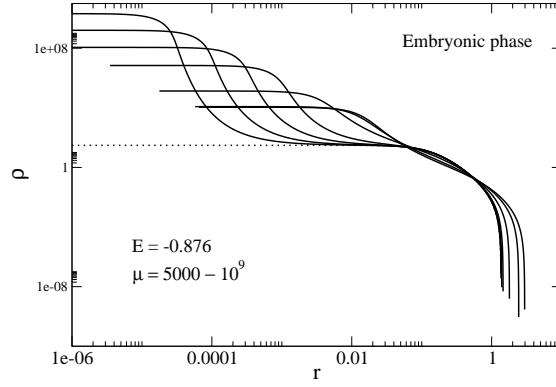


Figure 16: Density profile of the embryonic phase (solution B) for different values of μ in logarithmic scales (we have selected $\mu = 5000, 10^4, 10^5, 10^6, 10^7, 10^8$, and 10^9). For increasing μ , the solution B coincides with the solution A (gaseous phase; dotted line) corresponding to the classical King model, except that it contains a small embryonic degenerate nucleus with a small mass and a small absolute value of potential energy. This nucleus of almost constant density is followed by a plateau as detailed in [30].

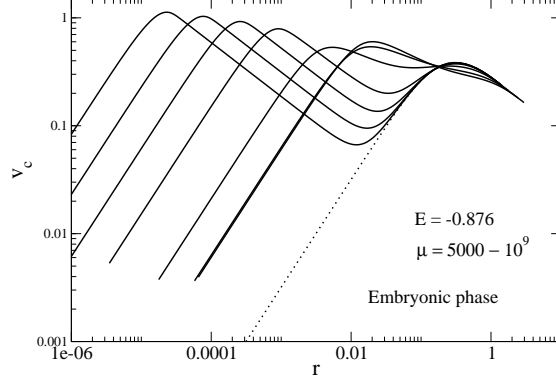


Figure 17: Circular velocity of the embryonic phase (solution B) for different values of μ in logarithmic scales. For increasing μ , the solution B approaches the solution A (gaseous phase; dotted line) corresponding to the classical King model, except at very small distances. The presence of a small nucleus (fermion ball) where $v_c \propto r$ followed by a plateau where $v_c \propto r^{-1/2}$ manifests itself by a secondary peak in the rotation curve at the very center of the system (see Fig. 18). However, these distances are probably not accessible to observations. Furthermore, these solutions are thermodynamically unstable so this secondary peak may not be physical.

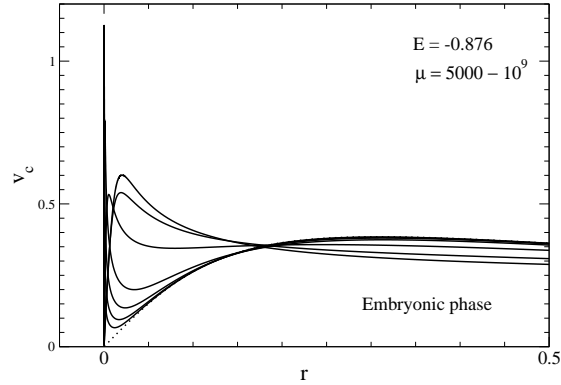


Figure 18: Circular velocity of the embryonic phase (solution B) for different values of μ in linear scales. For large values of μ , we recover the classical King model (dotted line) except at the very center. The secondary peak due to the degenerate nucleus (fermion ball) manifests itself by a spike near the origin.

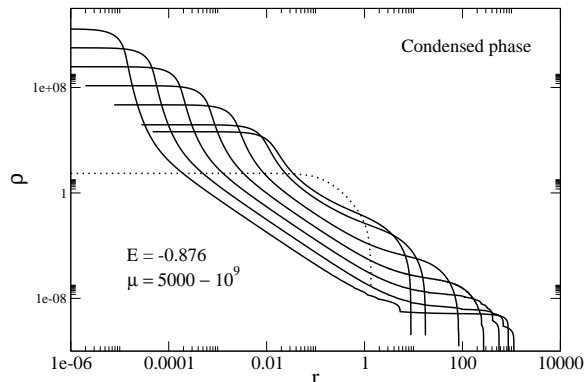


Figure 19: Density profile of the condensed phase (solution C) for different values of μ in logarithmic scales. For increasing values of μ , the solution C contains a small degenerate nucleus with a relatively small mass but a more and more negative potential energy. As a result, the halo becomes hotter and hotter in order to conserve the total energy. This is why it forms a sort of plateau with constant density that extends at larger and larger distances. The resulting profile is very different from solution A (gaseous phase; dotted line) corresponding to the classical King model.

Fig. 15). Still, the two solutions A and B are physically distinct. In particular, the solution B is unstable as further discussed in Sec. 7.

The solution C (condensed phase) is very different from the solution A (gaseous phase) and from the solution B (embryonic phase). Like solution B, it has a nucleus-halo structure. It contains a small degenerate nucleus that has a small mass and a small radius. However, unlike solution B it has a very negative potential energy. As a result, the halo must be very hot in order to conserve the total energy. This is why β_C is small (see Fig. 15). Since the halo is hot, it expands at very large distances (see Figs. 19-21). The halo radius increases as μ increases. For $\mu \rightarrow +\infty$, the mass and the radius of the nucleus tend to zero but its potential energy tends to $-\infty$. As a result, the temperature of the halo tends to $+\infty$ and its radius also tends to $+\infty$. We therefore obtain a singular structure similar to the “binary + hot halo” mentioned in the Introduction (see footnote 3). For finite μ , quantum mechanics provides a regularization of this singular structure: the “binary” is replaced by a “fermion ball” whose size is fixed by quantum mechanics.

We now consider the effect of starting from the gaseous phase, and decreasing the energy below the critical energy E_c . This is a natural evolution since the energy $E(t)$ decreases, and the concentration parameter $k(t)$ increases, as the system slowly evaporates [17]. When $E < E_c$, the system undergoes a gravitational collapse towards the condensed phase (solution C). According to the preceding discussion, the result of the gravitational collapse is to form a

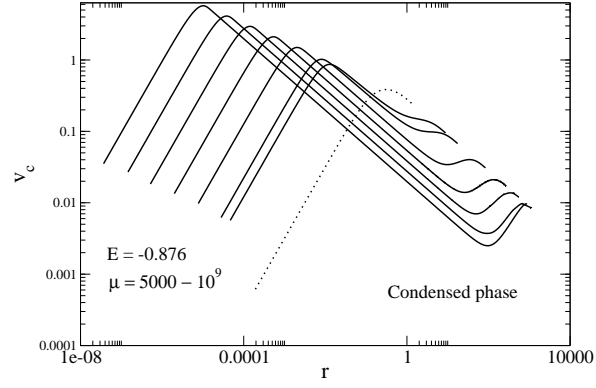


Figure 20: Circular velocity of the condensed phase (solution C) for different values of μ in logarithmic scales. It is very different from solution A (gaseous phase; dotted line) corresponding to the classical King model. This is because the halo is expelled at large distances as the nucleus becomes denser and denser, and more and more energetic.

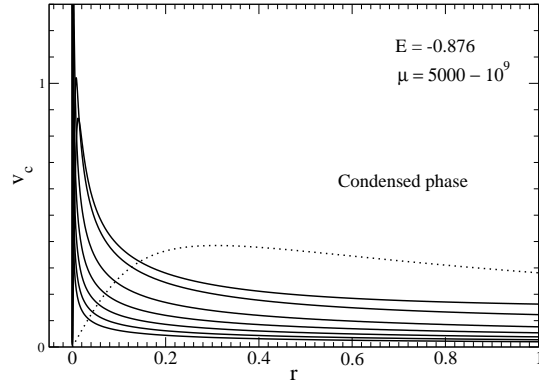


Figure 21: Circular velocity of the condensed phase (solution C) for different values of μ in linear scales.

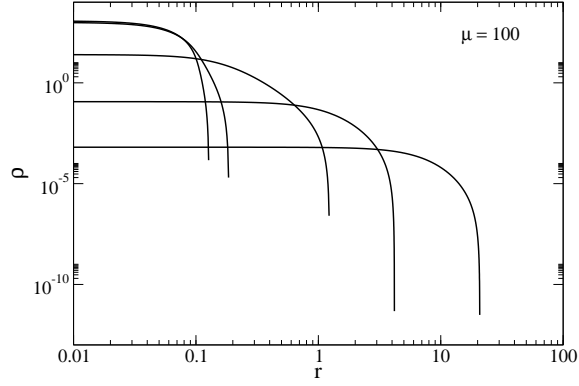


Figure 22: Density profile along the series of equilibria for $\mu = 100$ in logarithmic scales. We have selected $k = 0.142$ ($E = -0.0329$, $\beta = 0.993$), $k = 1.31$ ($E = -0.181$, $\beta = 1.66$), $k = 4.99$ ($E = -0.914$, $\beta = 1.03$), $k = 18.0$ ($E = -4.27$, $\beta = 1.03$), and $k = 41$ ($E = -4.65$, $\beta = 2.51$).

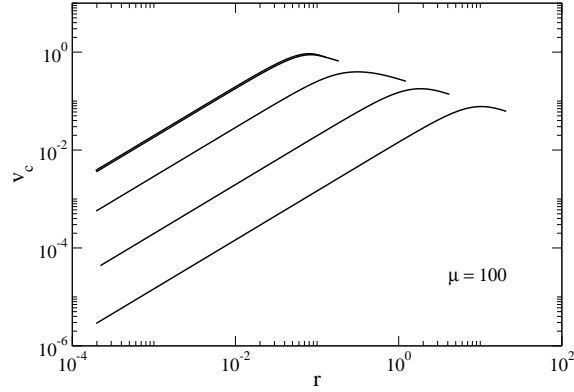


Figure 23: Circular velocity along the series of equilibria for $\mu = 100$ in logarithmic scales. We have selected $k = 0.142$, $k = 1.31$, $k = 4.99$, $k = 18.0$, and $k = 41$.

degenerate nucleus (fermion ball) of much smaller mass than the initial cluster and to expel a hot and massive envelope at very large distances.¹¹ This is similar to the formation of red-giants and to the supernova explosion phenomenon, except that it takes considerably much more time (of the order of the Hubble time!) since the gravothermal catastrophe is a rather slow process. At the end, since the envelope is expelled, only the degenerate nucleus remains. This could be a mechanism of formation of dwarf dark matter halos that are completely degenerate.

We would like to point out that the previous results are valid for large values of μ (large halos). For small values of μ (small halos), and in particular for $\mu < \mu_{MCP} = 1980$, the series of equilibria unwinds and all the King profiles are stable. In that case, there is no phase transition (no collapse) anymore. The King profiles in the region of negative specific heat have a core-halo structure but the distinction between the degenerate core and the halo is not clear-cut (see Figs. 22 and 23). These solutions may describe dwarf and intermediate size halos where degeneracy effects are important.

7 Can large dark matter halos harbor a fermion ball?

Many observations have revealed that galaxies and dark matter halos contain a very massive object at the center. This compact object is usually interpreted as a black hole. Alternatively, some authors have suggested that this object could actually be a fermion ball made of the same matter as the rest of the halo. Indeed, some configurations of the self-gravitating Fermi gas at finite temperature have a nucleus-halo structure resembling a large dark matter halo with a small compact object at the center. This nucleus-halo structure is particularly clear in the embryonic phase (solution B). These solutions are similar to the gaseous phase (solution A) except that they contain a small degenerate nucleus. The halo is similar to a truncated classical isothermal gas consistent with the observations of large dark matter halos (Burkert profile) and the nucleus has the form of a degenerate fermion ball. When μ is large, the fermion ball is very small so it does not affect the structure of the halo. The corresponding density profiles and rotation curves are represented in Figs. 16-18. The nucleus creates a secondary peak and a dip in the rotation curve at very small radii that may not be resolved observationally. This type of nucleus-halo configurations has been obtained by several authors [40, 30, 41, 25]. Some of them [41] made the interesting suggestion that the fermion ball could mimic the effect of a central black hole. However, these authors [41] did not investigate the stability of such configurations. Our study (see also [30, 42, 25]) shows that these structures (solution B) are thermodynamically unstable (*i.e.* unreachable) because they

¹¹Things are very different in the canonical ensemble. For $T < T_c$ the system collapses and forms a degenerate nucleus containing most of the mass. In that case, there is almost no atmosphere. The core-halo structure is a property of the microcanonical ensemble that is not present in the canonical ensemble [25].

are saddle points of entropy at fixed mass and energy. Therefore, large dark matter halos should not contain a degenerate nucleus (fermion ball). This is an important prediction of our study. The fact that fermion balls are not observed at the center of galaxies (a central black hole is indeed observationally favored over a fermion ball [43, 44]) is in agreement with our result.

We note that the solutions of the condensed phase (solution C) also have a core-halo structure with a degenerate nucleus and a non degenerate envelope. These solutions are stable. However, in that case, the nucleus formed by gravitational collapse releases an enormous energy that heats the envelope and disperse it at very large distances. As a result, only the degenerate object remains at the end. These solutions do not resemble a large dark matter halo with a central nucleus because the atmosphere is too hot (compare solutions B and C in Figs. 16-21). However, the nucleus alone resembles a dwarf halo that is a completely degenerate object without atmosphere.

8 Can large dark matter halos harbor a black hole?

We have seen in the previous section that the presence of a fermion ball at the center of large dark matter halos is unlikely because these nucleus-halo structures are unreachable: they are saddle points of entropy. The presence of a central black hole is more likely [43, 44]. These black holes could be formed by the mechanism discussed by Balberg *et al.* [8] if dark matter is collisional. In that case, large dark matter halos may undergo a gravothermal catastrophe when $E < E_c$. The increase of the density and temperature of the core during the collapse can trigger a dynamical (Vlasov) instability of general relativistic origin leading to the formation of a central black hole. During this process, only the core collapses. This can form a black hole of large mass without affecting the structure of the halo. Therefore, this process leads to large halos compatible with the Burkert profile for $r > 0$ (see Sec. 4) but harboring a central black hole at $r = 0$.

In this scenario, the presence of black holes at the center of dark matter halos is conditioned by the possibility that dark matter halos may undergo a gravothermal catastrophe. Now, when quantum mechanics is taken into account, as in the fermionic King model, an important result of our study is the existence of a microcanonical critical point $\mu_{MCP} = 1980$ below which the microcanonical phase transition (gravothermal catastrophe) is suppressed. Roughly speaking, this result implies that “large” dark matter halos ($\mu > \mu_{MCP}$) that are non degenerate can undergo a gravothermal catastrophe (although this is not compulsory¹²) and contain a central black hole while “small” dark matter halos ($\mu < \mu_{MCP}$) that are quantum objects stabilized by the Pauli exclusion

¹²It is possible that a proportion of large dark matter halos have a concentration parameter $k < k_{MCE}$ and have not undergone core collapse (these halos do not contain a black hole) while some halos have reached the critical threshold $k = k_{MCE}$ and have undergone core collapse (these halos contain a black hole).

principle cannot contain a central black hole because they do not experience a gravothermal catastrophe. This result seems to qualitatively agree with the observations.

9 A scenario of formation of dark matter halos

We sketch below a general scenario of formation of dark matter halos assuming that they are made of fermions such as massive neutrinos.

Initially, dark matter can be considered as a spatially homogeneous gas described by the relativistic Fermi distribution $f = \eta_0^{Pauli} / (1 + e^{pc/k_B T})$ where $\eta_0^{Pauli} = gm^4/h^3$ is the Pauli bound [45]. The maximum value of the distribution function is $f_0 = (1/2)\eta_0^{Pauli} = (g/2)m^4/h^3$. Since this gas is collisionless, it is described by the Vlasov-Poisson system. A spatially homogeneous distribution is unstable and undergoes gravitational collapse (Jeans instability). The fermionic Jeans wavenumber $k_J = \sqrt{12\pi G}(8\pi/3)^{1/3}m^{4/3}\rho^{1/6}/h$ [28] is finite so that quantum mechanics prevents the formation of small-scale structures and fixes a ground state. This produces a sharp cut-off in the power spectrum.¹³ In the linear regime, some regions of over-density form. When the density has sufficiently grown, these regions collapse under their own gravity at first in free fall. Then, as nonlinear gravitational effects become important at higher densities, these regions undergo damped oscillations (due to an exchange of kinetic and potential energy) and finally settle into a quasi stationary state (QSS) on a coarse-grained scale. This corresponds to the process of violent relaxation first reported by Lynden-Bell [6] for stellar systems like elliptical galaxies. This process is related to phase mixing and nonlinear Landau damping. It is applied here to dark matter. In this context, the QSSs represent dark matter halos. Because of violent relaxation, the halos are almost isothermal and have a core-halo structure. The density of the core is relatively large and can reach values at which quantum effects or Lynden-Bell's type of degeneracy are important.¹⁴ On the other hand, the halo is relatively hot and behaves more or less as a classical isothermal gas. Actually, it cannot be exactly isothermal otherwise it would have an infinite mass. The finite extension of the halo may be due to incomplete violent relaxation [6]. The extension of the halo may also be limited by tidal effects. In that case, the complete configuration of the system can be described by the fermionic King model [27]. As we have demonstrated, the fermionic King model can show a wide diversity of configurations with different degrees

¹³In the CDM model where $c_s^2 = p'(\rho) = k_B T/m \rightarrow 0$, the classical Jeans wavenumber $k_J = \sqrt{4\pi G\rho}/c_s \rightarrow +\infty$. Therefore, if this model were valid, the spatially homogeneous gas would be unstable at all wavelengths and, consequently, structures would form at all scales. Since there is no ground state, we would observe dark matter halos of all sizes. The fact that we do not observe halos below a certain scale (missing satellite problem) shows that quantum mechanics must be taken into account in dark matter. Another possibility is to consider warm dark matter (WDM) with $T \neq 0$. In that case, the Jeans wavenumber k_J and the maximum value of the distribution function f_0 are determined by thermal effects (*i.e.* by the velocity dispersion of the particles).

¹⁴In the case of dark matter, the Lynden-Bell bound and the Pauli bound are of the same order, differing by a factor two, since $\eta_0^{LB} = f_0 \sim \eta_0^{Pauli}/2 = (g/2)m^4/h^3$.

of nuclear concentration. The system can be everywhere non degenerate, everywhere completely degenerate, or have a core-halo structure with a degenerate core and a non degenerate halo. Small halos, that are compact, are degenerate. Their flat core is due to quantum mechanics. Assuming that the smallest and most compact observed dark matter halo of mass $M_h = 0.39 \cdot 10^6 M_\odot$ and radius $r_h = 33 \text{ pc}$ (Willman 1) is completely degenerate ($T = 0$) leads to a fermion mass of the order of $1.23 \text{ keV}/c^2$ [46, 28]. These particles may be sterile neutrinos. Small halos can merge with each other to form larger halos. This is called hierarchical clustering. The merging of the halos also corresponds to a process of collisionless violent relaxation. Large halos, that are dilute, are non degenerate. Their flat core is due to thermal effects.¹⁵ Knowing the mass of the fermions, we can deduce from the observations that halos of mass $0.39 \cdot 10^6 M_\odot < M_h < 2.97 \cdot 10^6 M_\odot$ are quantum (degenerate) objects while halos of mass $M_h > 2.97 \cdot 10^6 M_\odot$ are classical (non degenerate) objects [46, 28]. In the classical limit, numerical simulations of violent relaxation generically lead to configurations presenting an isothermal core and a halo whose density decreases as $r^{-\alpha}$ with $\alpha = 4$ [4, 47, 48, 49]. These configurations are relatively close to Hénon's isochrone profile. They can be explained by models of incomplete violent relaxation [50, 51, 52]. A density slope $\alpha = 4$ is also consistent with a King profile of concentration $k \sim 5$ [28]. If the halos were truly collisionless, they would remain in a virialized configuration. However, if the core is dense enough, collisional effects can come into play and induce an evolution of the system on a long timescale (driven by the gradient of temperature -velocity dispersion- between the core and the halo) during which the concentration parameter $k(t)$ increases while the slope $\alpha(t)$ of the density profile decreases much like in globular clusters [17]. We now have to distinguish between small halos of mass $M_h < 1.60 \cdot 10^7 M_\odot$ (corresponding to $\mu < \mu_{MCP} = 1980$) and large halos of mass $M_h > 1.60 \cdot 10^7 M_\odot$ (corresponding to $\mu > \mu_{MCP}$) [28]. For small halos, the series of equilibria (see Fig. 12) does not present any instability so that $k(t)$ increases and $\alpha(t)$ decreases regularly due to collisions and evaporation. These halos are degenerate. They are stabilized against gravitational collapse by quantum mechanics. As a result, they do not experience the gravothermal catastrophe so they should not contain black holes. For large halos, the series of equilibria (see Fig. 8) presents an instability at $k_{MCE} = 7.44$. Because of collisions and evaporation, the concentration parameter increases from $k \sim 5$ corresponding to a density slope $\alpha = 4$ (a typical outcome of violent relaxation) up to the critical value $k_{MCE} = 7.44$ corresponding to a density slope $\alpha \sim 3$. Less steep halos ($\alpha < 3$) are unstable ($k > k_{MCE}$). Large halos are expected to be close to the point of marginal stability (see solution A in Fig. 9). At that point, the King profile can be approximated by the modified Hubble profile that is relatively close to the Burkert profile fitting observational halos. Some halos may be stable ($k < k_{MCE}$) but some halos may undergo a gravothermal catastrophe ($k > k_{MCE}$). In that case, they experience core collapse. The evolution is self-similar. The system develops an isothermal core surrounded by a halo

¹⁵Here, the temperature is effective and it must be understood in the sense of Lynden-Bell.

with a density slope $\alpha = 2.2$ [17, 8]. The core radius decreases with time while the central density and the central temperature increase. The halo does not change. The specific heat of the core is negative. Therefore, by losing heat to the profit of the halo, the core grows hotter and enhances the gradient of temperature with the halo so the collapse continues. This is the origin of the gravothermal catastrophe [10]. For weakly collisional classical systems (globular clusters), core collapse leads to a finite time singularity with a density profile $\rho \propto r^{-2.2}$ at $t = t_{coll}$. The singularity has infinite density but contains no mass. It corresponds to a tight binary surrounded by a hot halo [17]. However, for collisional dark matter halos, the situation is different. If the particles are fermions, and if the mass of the halo is not too large ($\mu > \mu_{MCP}$ not too large), the gravothermal catastrophe stops when the core of the system becomes degenerate. This leads to a configuration with a small degenerate nucleus (condensed state) surrounded by an extended atmosphere that is relatively different from the structure of the halo before collapse (see solution C in Figs. 9 and 19). However, the formation of this equilibrium structure can be very long (of the order of the Hubble time) so that, on an intermediate timescale, the system is made of a contracting fermion ball surrounded by an atmosphere that is not too much affected by the collapse of the nucleus. Alternatively, if the halo mass is large ($\mu > \mu_{MCP}$ large), during the gravothermal catastrophe the system can develop a (Vlasov) dynamical instability of general relativistic origin and form a central black hole without affecting the structure of the halo [8]. In this way, the system is similar to the halo before collapse (Burkert profile) except that it contains a central black hole.¹⁶ Large halos should not contain a fermion ball because these nucleus-halos structures (see solution B in Figs. 9 and 16) are unreachable (saddle point of entropy).

10 On the collapse of large dark matter halos

In this section, we come back on the different scenarios concerning the possible collapse of large dark matter halos (when $\mu > \mu_{MCP} = 1980$ and $E < E_c$) and on their resulting structure.

One possibility is that the collapse below E_c leads to a core-halo configuration with a dense and compact degenerate core (fermion ball), similar to a white dwarf star at $T = 0$, surrounded by a hot atmosphere. Actually, the atmosphere is so hot that it has the tendency to be expelled at large distances.

¹⁶More precisely, the core collapse of fermionic dark matter halos is a two-stages process. In a first stage [8], the core collapses while the halo does not change. Only the density, the radius and the temperature of the core change. This creates strong gradients of temperature between the core and the halo. At sufficiently high temperatures (achievable if μ is large) the system becomes relativistic and triggers a dynamical instability leading to a black hole with a large mass. Alternatively, if μ is small, quantum mechanics can stop the increase of the central density and central temperature before the system enters in the relativistic regime. In that case, core collapse stops. Then, in a second stage (never studied until now because it requires quantum simulations), the temperature uniformizes between the core and the halo. Therefore, the halo heats up and extends at large distances until an equilibrium state with a uniform temperature T is reached (see solution C in Figs. 9 and 19).

This is reminiscent of the red-giant phase where a star, having exhausted its nuclear fuel, collapses into a white dwarf star and ejects its outer layers by forming a planetary nebula. This is also reminiscent of the supernovae explosion phenomenon [53] leading to a degenerate compact object such as a neutron star or a black hole and to the expulsion of a massive envelope. We may wonder whether a similar scenario can take place (or has already taken place!) at the galactic scale. We may speculate that many large dark matter halos are close to stable classical King models with $k < k_{MCE}$ but that some halos may reach the critical value $k = k_{MCE}$ and collapse to give birth to degenerate dwarf dark matter halos of much smaller mass, with the expulsion of a massive envelope. We emphasize, however, that this phenomenon takes considerably much more time (of the order of the Hubble time) than the supernova phenomenon (a few seconds) since the gravothermal catastrophe is a rather slow process.

Another possibility is that the collapse below E_c leads to the formation of a black hole before quantum mechanics comes into play. In that case, we predict [28] that large dark matter halos with mass $M_h > 1.60 \cdot 10^7 M_\odot$ may contain a central black hole because they are non degenerate and can undergo a gravothermal catastrophe ($\mu > \mu_{MCP} = 1980$) while intermediate size and dwarf dark matter halos with mass $M_h < 1.60 \cdot 10^7 M_\odot$ should not contain a central black hole because they are stabilized by quantum mechanics and cannot undergo a gravothermal catastrophe ($\mu < \mu_{MCP} = 1980$).

Finally, one could imagine that the collapse of dark matter halos leads to a fermion ball that could mimic the effect of a central black hole. However, one important conclusion of our study is that large dark matter halos should *not* contain a degenerate nucleus (fermion ball) because these nucleus-halo configurations are thermodynamically unstable (saddle points of entropy). Therefore, they should be unreachable.

11 Conclusion

In this contribution, we have described some thermodynamical properties of the fermionic King model introduced in [26, 27]. A more detailed study is presented in [28]. The interest of this distribution function with respect to statistical mechanics was pointed out in [25]: (i) this distribution has a finite mass, so there is no need to enclose the system within an artificial box; (ii) due to the exclusion constraint, there exist an equilibrium state for all accessible energies; (iii) this model exhibits interesting phase transitions between gaseous and condensed states similar to those described in [25] for a gas of self-gravitating fermions enclosed within a box.

The fermionic King model also provides a realistic model of dark matter halos. Dwarf dark matter halos of mass $M_h = 0.39 \cdot 10^6 M_\odot$ are quantum objects. They are completely degenerate and represent the ground state of the sequence of dark matter halos. This fixes the mass of the fermions to about $1.23 \text{ keV}/c^2$. Intermediate size halos of mass $0.39 \cdot 10^6 M_\odot < M_h < 2.97 \cdot 10^6 M_\odot$ are partially degenerate. Large dark matter halos of mass $M_h > 2.97 \cdot 10^6 M_\odot$

are non-degenerate so the classical King model can be used. Many large halos seem to be close to the limit of marginal stability in MCE ($k \sim k_{MCE}$). The corresponding King profile can be approximated by the modified Hubble profile. It has a flat core and a halo in which the density decreases as r^{-3} . The modified Hubble profile is relatively close to the empirical Burkert profile that fits several rotation curves of galaxies. Some halos may have undergone the gravothermal catastrophe ($k > k_{MCE}$). Two possibilities can happen. Core collapse may be stopped by quantum mechanics. In that case, the system forms a degenerate object and expels a hot and massive envelope. This could be a mechanism responsible for the formation of dwarf halos that are completely degenerate. Another possibility is that the collapse triggers a dynamical instability of general relativistic origin. In that case, the system forms a central black hole without affecting the halo. This could be the mechanism responsible for the presence of black holes at the center of galaxies. In order to form a black hole, the halo mass must be sufficiently large ($M_h > 1.60 \cdot 10^7 M_\odot$) so that the gravothermal catastrophe can take place ($\mu > \mu_{MCP}$). Small halos ($M_h < 1.60 \cdot 10^7 M_\odot$) should not contain black holes because they do not experience the gravothermal catastrophe ($\mu < \mu_{MCP}$). Therefore, the presence (or absence) of black holes at the center of galaxies may be connected to the existence of a microcanonical critical point ($\mu_{MCP} = 1980$) in the fermionic King model [28]. Finally, we have shown that the presence of fermion balls at the center of dark matter halos is unlikely because these nucleus-halo structures are unreachable (saddle points of entropy). This may explain why black holes at the center of galaxies are observationally favored over fermion balls [43, 44].

Obviously, several configurations of dark matter halos are possible within the fermionic King model making the study of this model very rich. The system can be non degenerate (large halos), partially degenerate (intermediate size halos), or completely degenerate (dwarf halos). We can obtain core-halo configurations with a wide diversity of nuclear concentration depending on μ (*i.e.* the size of the system) and E . This may account for the diversity of dark matter halos observed in the universe. Large dark matter halos are non degenerate classical objects. They may contain a black hole. Small halos are degenerate quantum objects. They should not contain a black hole. Our approach is the first attempt to determine the caloric curves of dark matter halos. This allows us to study the thermodynamical stability of the different configurations and to reject those that are unstable. In particular, we have shown that the nucleus-halo configurations considered in the past (as in Fig. 16) are unstable. More work is needed to relate our theoretical results to the observations.

References

- [1] J. Binney, S. Tremaine *Galactic Dynamics* (Princeton Series in Astrophysics, 2008)
- [2] J.F. Navarro, C.S. Frenk, S.D.M. White, *Astrophys. J.* **462**, 563 (1996)

- [3] A. Burkert, *Astrophys. J. Lett.* **447**, L25 (1995)
- [4] M. H  non, *Ann. Astrophys.* **27**, 83 (1964)
- [5] I.R. King, *Astron. J.* **71**, 64 (1966)
- [6] D. Lynden-Bell, *Mon. Not. R. Astron. Soc.* **136**, 101 (1967)
- [7] D.N. Spergel, P.J. Steinhardt, *Phys. Rev. Lett.* **84**, 1 (2000)
- [8] S. Balberg, S.L. Shapiro, S. Inagaki, *Astrophys. J.* **568**, 475 (2002)
- [9] V.A. Antonov, *Vest. Leningr. Gos. Univ.* **7**, 135 (1962); Translation in *IAU Symposium* **113**, 525 (1985)
- [10] D. Lynden-Bell, R. Wood, *Mon. Not. R. Astron. Soc.* **138**, 495 (1968)
- [11] C. Sire, P.H. Chavanis, *Phys. Rev. E* **66**, 046133 (2002)
- [12] R.W. Michie, *Mon. Not. R. Astron. Soc.* **125**, 127 (1963)
- [13] I.R. King, *Astron. J.* **70**, 376 (1965)
- [14] R. Emden, *Gaskugeln* (Teubner Verlag, Leipzig, 1907)
- [15] P.H. Chavanis, *Astron. Astrophys.* **432**, 117 (2005)
- [16] P.H. Chavanis, *Astron. Astrophys.* **556**, A93 (2013)
- [17] H. Cohn, *Astrophys. J.* **242**, 765 (1980)
- [18] D. Lynden-Bell, P.P. Eggleton, *Mon. Not. R. Astron. Soc.* **191**, 483 (1980)
- [19] D. Heggie, D. Stevenson, *Mon. Not. R. Astron. Soc.* **230**, 223 (1988)
- [20] M. H  non, *Ann. Astrophys.* **24**, 369 (1961)
- [21] M. H  non, *Ann. Astrophys.* **28**, 62 (1965)
- [22] S. Inagaki, D. Lynden-Bell, *Mon. Not. R. Astron. Soc.* **205**, 913 (1983)
- [23] D. Sugimoto, E. Bettwieser, *Mon. Not. R. Astron. Soc.* **204**, 19 (1983)
- [24] D. Heggie, N. Ramamani, *Mon. Not. R. Astron. Soc.* **237**, 757 (1989)
- [25] P.H. Chavanis, *Int. J. Mod. Phys. B* **20**, 3113 (2006)
- [26] R. Ruffini, L. Stella, *Astron. Astrophys.* **119**, 35 (1983)
- [27] P.H. Chavanis, *Mon. Not. R. Astron. Soc.* **300**, 981 (1998)
- [28] P.H. Chavanis, M. Lemou, F. M  hats, arXiv:1409.7838 and 1409.7840
- [29] H.J. de Vega, P. Salucci, N.G. Sanchez, *Mon. Not. R. Astron. Soc.* **442**, 2717 (2014)

- [30] P.H. Chavanis, J. Sommeria, Mon. Not. R. Astron. Soc. **296**, 569 (1998)
- [31] J. Katz, Mon. Not. R. Astron. Soc. **190**, 497 (1980)
- [32] T. Padmanabhan, Phys. Rep. **188**, 285 (1990)
- [33] J. Katz, Found. Phys. **33**, 223 (2003)
- [34] M. Lemou, F. Méhats, P. Raphaël, Invent. Math. **187**, 145 (2012)
- [35] L. Casetti, C. Nardini, Phys. Rev. E **85**, 061105 (2012)
- [36] S. Chandrasekhar, *An Introduction to the Study of Stellar Structure* (Dover, 1958)
- [37] M. Hénon, Ann. Astrophys. **22**, 126 (1959)
- [38] C. Sire, P.H. Chavanis, Phys. Rev. E **69**, 066109 (2004)
- [39] J. Katz, Mon. Not. R. Astron. Soc. **183**, 765 (1978)
- [40] J.G. Gao, M. Merafina, R. Ruffini, Astron. Astrophys. **235**, 1 (1990)
- [41] N. Bilic, F. Munyaneza, G.B. Tupper, R.D. Viollier, Prog. Part. Nucl. Phys. **48**, 291 (2002)
- [42] P.H. Chavanis, Phys. Rev. E **65**, 056123 (2002)
- [43] R. Schödel *et al.*, Nature **419**, 694 (2002)
- [44] M.J. Reid, Int. J. Mod. Phys. D **18**, 889 (2009)
- [45] S. Tremaine, J.E. Gunn, Phys. Rev. Lett. **42**, 407 (1979)
- [46] C. Destri, H.J. de Vega, N.G. Sanchez, New Astronomy **22**, 39 (2013)
- [47] T.S. van Albada, Mon. Not. R. Astron. Soc. **201**, 939 (1982)
- [48] F. Roy, J. Perez, Mon. Not. R. Astron. Soc. **348**, 62 (2004)
- [49] M. Joyce, B. Marcos, F. Sylos Labini, Mon. Not. R. Astron. Soc. **397**, 775 (2009)
- [50] G. Bertin, M. Stiavelli, Astron. Astrophys. **137**, 26 (1984)
- [51] M. Stiavelli, G. Bertin, Mon. Not. R. Astron. Soc. **229**, 61 (1987)
- [52] J. Hjorth, J. Madsen, Mon. Not. R. Astron. Soc. **253**, 703 (1991)
- [53] Y. Pomeau, M. Le Berre, P.H. Chavanis, B. Denet, Eur. Phys. J. E **37**, 26 (2014)